PATHOLOGY
RESEARCH AND
PRACTICE

Pathology of Visceral Organs and Bone Marrow in an Acid Sphingomyelinase Deficient Knock-Out Mouse Line, Mimicking Human Niemann-Pick Disease Type A

A Light and Electron Microscopic Study

T. A. Kuemmel[1], J. Thiele[1], R. Schroeder[1] and W. Stoffel[2]

[1]Institute of Pathology and [2]Neuroscience Laboratory, Institute of Biochemistry, Medical Faculty, University of Cologne, Cologne, Germany

Summary

A recently generated aSmase knock-out mouse line develops a lethal storage disease which mimics the neurovisceral form of Niemann-Pick disease in man. In extension to the previously described neuropathological changes, the purpose of this study was to provide a detailed morphological, particularly ultrastructural analysis of the visceral organs of these animals including spleen, liver, intestine, lung, and kidney along with a sequential histological investigation of the bone marrow. Our results showed a progressive lysosomal storage as indicated by an increasing amount of foam cells in the bone marrow with age, extending to all visceral organs. Most severe storage phenomena were found in the mononuclear-macrophage system, however, parenchymal cells of visceral organs were also markedly involved. The ultrastructural appearance of membrane-bound inclusions displayed a pleomorphic aspect ranging from small vesicular and vesiculo-granular structures to huge lysosomes with membranous material deposited in lamellar or stacked arrays. The obvious similarity to its human counterpart along with an easy availability makes this animal model a valuable tool for further studies of Niemann-Pick disease type A.

Key words: Knock-out mouse – Niemann-Pick disease – Visceral organs – Bone marrow – Ultrastructure

Introduction

It is generally accepted that Niemann-Pick (NP) disease belongs to the family of lysosomal storage disorders and includes several subtypes. Type A (NP-A), the neurovisceral form and type B (NP-B), the visceral form, are caused by a complete or incomplete loss of the enzyme acid sphingomyelinase (aSmase). Type C (NP-C) is mainly characterized by an intracellular cholesterol storage, but the underlying defect has not yet been understood in detail [2, 11, 36]. Only recently could a gene involved in the latter disorder be identified, revealing a homology to mediators of cholesterol homeostasis [5]. However, a closer look at the pertinent literature reveals a striking discrepancy in regard to the number of studies dealing with NP-C compared to those referring to the aSmase-deficient disorder. Among other reasons, this paucity may be attributed to the lack of an appropriate animal model of the latter subtype rather than reflect its incidence [32]. In this context, several mouse strains mimicking human NP-C have been recruited and extensively investigated [25, 27]. These murine models, arising from spontaneous mutations disclosed a defect in the recently isolated Niemann-Pick gene [21]. On the other hand, there are only anecdotal reports of NP-A-like conditions in animals that are clearly characterized by aSmase deficiency, i.e. in a poodle dog [4] and in several feline species [38, 39]. This serious setback for the study of NP disease was recently overcome by the generation of two aSmase-deficient knock-out mouse strains [15, 26]. For this purpose, the aSmase gene of wild type mice, in which exon

0344-0338/97/0193-0663$5.00/0

III had been disrupted, was used for gene targeting by homologous recombination in embryonic stem cells. Previous studies of the latter model, regarding biochemistry (complete loss of aSmase activity) and the characteristic lesions of the central and peripheral nervous systems [19] clearly indicated its close resemblance to the neurovisceral form of human NP disease. In extension to these neuropathological findings the present study is focused on a sequential investigation of storage phenomena in the bone marrow and additionally, on an ultrastructural characterization of the peculiar changes occurring in the visceral organs of the so-called NP-mouse (NPM).

Material and Methods

Animals

We observed a total of eight mice. These included six aSmase$^{-/-}$ animals, two mice at day 140 of age, one mouse at day 18, 30, 50, 80 and two C57BL/6 control mice (day 18 and day 140 after birth). 140-day-old aSmase$^{-/-}$ mice revealed the full-blown clinical picture, characterized by generalized tremor, distinctive ataxia, hepatosplenomegaly and severe pulmonary distress.

Processing for Light and Electron Microscopic Analysis

Wild type and aSmase$^{-/-}$ mice were euthanized using CO_2 atmosphere and perfusion was conducted from the left ventricle using 20 ml of a mixture of 3% glutaraldehyde and 2% formaldehyde in 0.1 M phosphate buffered saline (PBS), pH 7.4. Bone marrow specimens derived from femur and spine underwent further fixation in an aldehyde solution (2 ml 25% glutaraldehyde, 3 ml 37% formaldehyde, 1.58 g calcium acetate in 100 ml distilled water) for 24 hrs at 4 °C. Representative tissue samples taken from spleen, liver, small intestine, lung and kidney were additionally fixed for 24 hrs at 4 °C either with 4% formaldehyde followed by embedding in paraffin wax or with 2.5% glutaraldehyde in 0.1 M sodium cacodylate buffer followed by processing for Araldite embedding. Paraffin-embedded specimens were sectioned at 5 µm and stained with hematoxylin-eosin and periodic acid-Schiff (PAS).

For Araldite embedding of visceral organ samples, fixed tissue blocks (0.5–1 mm^3) were rinsed in 0.1 M sodium cacodylate buffer and postfixed with 1% osmium tetroxide dissolved in the same buffer. After dehydration in graded ethanol, specimens were embedded in Araldite resin. Semithin sections (about 1.5 µm) of all specimens were mounted on glass slides and stained at 70 °C with an aqueous solution of 0.5% methylene blue in 0.5% borax/azure blue II. Ultrathin sections were mounted on 200 mesh nickel grids and stained by uranyl acetate and lead citrate. Grids were examined with the Zeiss EM 902a.

Results

Sequential examinations of bone marrow (day 18, 30, 50, 80, 140) in the aSmase-deficient mouse strain exhibited only few foam cells with onion-skin like appearance till day 50 of age. These displayed gross vacuolization of the cytoplasm and dislocation of nuclei towards the periphery (Fig. 1a). An obvious increase at day 80 and a high amount of foam cells at day 140 was evident (Fig. 1b). Moreover, a certain topographical vicinity of these cells towards osseous trabeculae (paratrabecular-endosteal and intermediate bone marrow compartment) could be observed (Fig. 1b). The staining of vacuolar inclusions with PAS was negative for macrophages in all organs under study.

Spleen tissue contained numerous foam cells, however, more frequently in the red than in the white pulp. An ultrastructural investigation revealed histiocytic cells that were packed with inclusions containing stacked or lamellar arranged membranous material of varying density besides electron lucent vacuoles that disclosed a tendency to fuse (Fig. 2a). Moreover, large foam cells were detected exhibiting heterogeneous deposits of membranous structures along with multivesicular or vesiculo-granular inclusions, sometimes disclosing fusion bodies of enormous size (Fig. 2b). Cytoplasmic organelles in these cells were almost completely replaced by lysosomes. Small foam cells, probably resulting from lymphocytic transformation, were infrequently detected in the white pulp of spleen (Fig. 2c), while lymphocytes often demonstrated one or few mostly electron lucent lysosomal bodies with little dispersed membranous material (Fig. 2d). Hematopoietic cells (granulocytes, normoblasts, megakaryocytes) did not show any storage phenomena.

A histological evaluation of liver in the NPM disclosed a distortion of the regular cellular architecture with appearance of numerous, focally clustered foam cells. These presented probably enlarged Kupffer cells that were localized in and partly occluded hepatic sinusoids throughout the liver without any topographical preference. Moreover, hepatocytes showed a distinctive cytoplasmic vacuolization. On ultrastructural evaluation they often displayed inclusions with predominantly stacked membranous material (Fig. 3a). Kupffer cells exhibited mostly membrane-bound inclusions, filled up with either loosely coiled or stacked membranous constituents (Fig. 3b). Moreover, single enlarged foam cells additionally showed multivesicular structures, partly with granular inclusions, and occasionally fusion bodies of enormous size occurred (Fig. 3c). The membrane-bound bodies in Kupffer cells were usually larger than those in hepatocytes.

Numerous giant foam cells were localized in the villous stroma of the small intestine and a sporadic vacuolization of epithelial cells was observed. Electron microscopy revealed these histiocytes of the lamina propria to contain membrane-bound bodies, preponderantly consisting of lamellar, concentrically arranged material. On the other hand, only few similar structures were detected in the intestinal epithelium (Fig. 3d).

By light microscopy, multiple giant alveolar macrophages harboring numerous vacuolar inclusions were identifiable in the lung, occasionally causing complete obstruction of alveoli. Ultrastructural evaluation revealed numerous membrane-bound bodies containing either loose, diffusely distributed electron dense material or membranous structures in concentric lamellar arrangement (Fig. 4a). Pneumocytes of type I and bronchiolar epithelia showed an identical pathology. Cytoplasmic vacuolar inclusions of these cells consisted of membranes without periodical arrangement. Moreover, small vesicular or confluent multivesicular structures could be observed which frequently harbored condensed membranous material forming osmiophilic granular inclusions (Fig. 4b, c). Pneumocytes of type II were unremarkable throughout (Fig. 4b). Fibrocytes of the alveolar septa and the bronchiolar connective tissue usually disclosed multivesicular bodies, often displaying an osmiophilic core (Fig. 4c).

Evaluation of paraffin histology and Araldite semithin sections of the renal tissue revealed a gross vacuolization of numerous glomerular and of epithelial cells in the proximal and distal tubules. This impression was extended by features of electron microscopy disclosing a similar pathology of mesangial cells and podocytes of glomeruli. Inclusions identified in these cells displayed an electron lucent vesicular appearance with confluence to some degree, often forming a dense nuclear core (Fig. 4d). The proximal and distal tubular epithelium frequently exhibited single or multiple membrane-bound bodies, with a concentric lamellar arrangement of varying size and density (Fig. 4e). Rarely, large multivesicular bodies, containing numerous electron lucent vesicles, often with an osmiophilic core, were observed in the tubular epithelium.

Vascular endothelial cells showed remarkable alterations in all visceral organs under study. These included an occurrence of numerous vesicular or vesiculo-granular bodies, that sometimes showed confluence and may contain loose membranous material, resulting in a narrowing of vascular lumina (Fig. 4a).

All pathologic features described above did not apply to age-matched control animals.

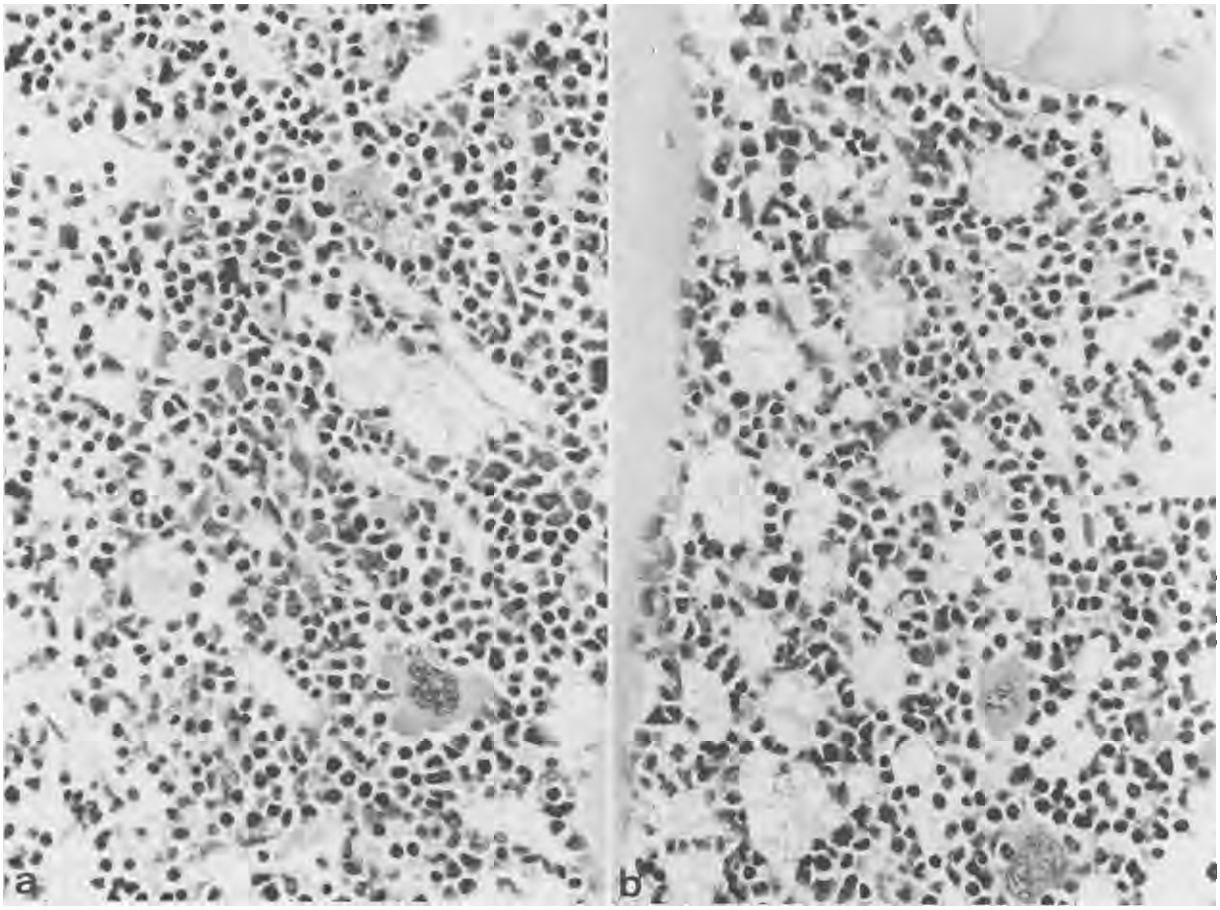

Fig. 1. Bone marrow in aSmase-deficient mice. **a)** 50-day-old animal displaying only few diffusely distributed foam cells. **b)** 140-days-old animal with numerous foam cells often located adjacent to osseous trabeculae. HE-staining, a, b: ×340.

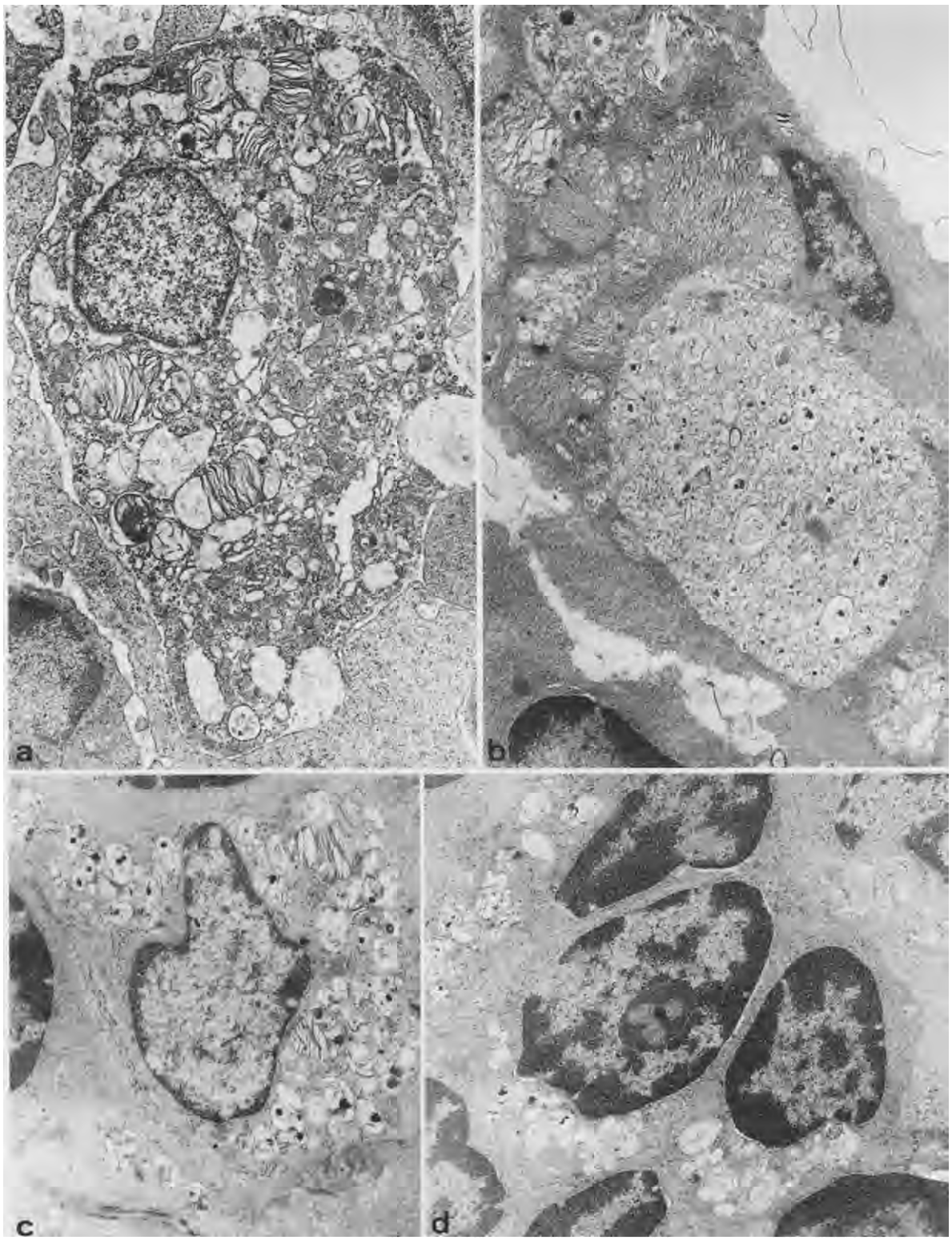

Fig. 2. Ultrastructure of spleen in a 140-day-old NPM. **a)** Histiocytic cell in a sinus of the red pulp disclosing membrane-bound bodies, filled with stacked membranous material along with electron lucent vacuoles that tend to fuse. **b)** Large foam cell in a splenal sinus with high pleomorphy of lysosomal inclusions replacing normal cell organelles. **c)** Small foam cell in the white pulp of spleen containing vesicular and vesiculo-granular inclusions besides lysosomal bodies with stacked membranous deposits. **d)** Lymphocyte of the white pulp with membrane-bound inclusions containing sparse membranous material. a–d: ×13,000.

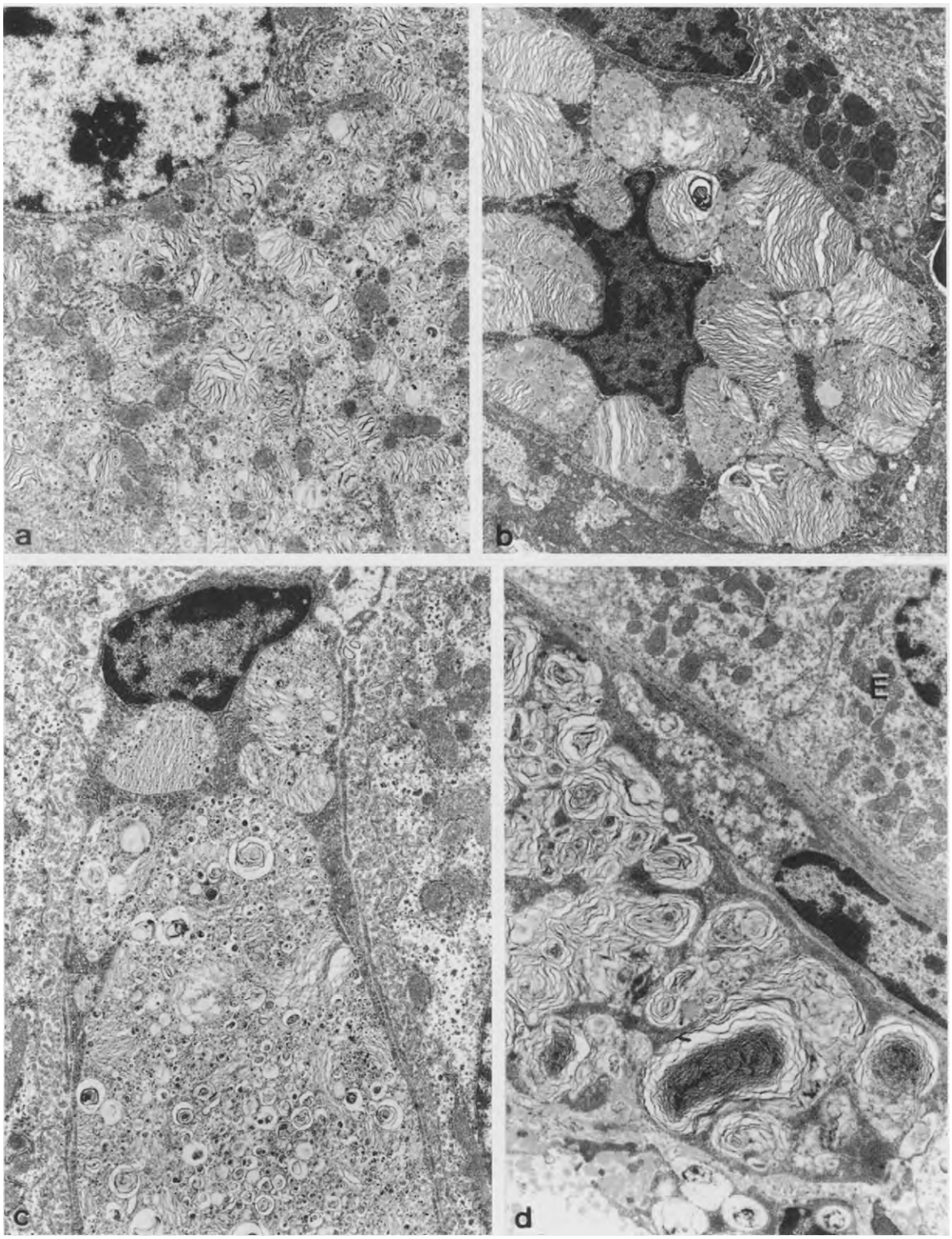

Fig. 3. Liver and small intestine of the 140-day-old NPM. **a)** Part of a hepatocyte containing numerous cytoplasmic inclusions with stacked membranous material. Mitochondria are normally shaped. **b)** Kupffer cell with huge lysosomal bodies harboring stacked membranous deposits that replace cytoplasmic organelles almost completely. **c)** Large foam cell with highly pleomorphic inclusions in its cytoplasm and marginal dislocated nucleus filling a hepatic sinusoid and occluding the space of Disse. **d)** Small intestine without visible lysosomes in the epithelium (E) but numerous large foam cells in the lamina propria displaying membranous material in typical concentric arrangement. a, b: ×6,000; c, d: ×9,200.

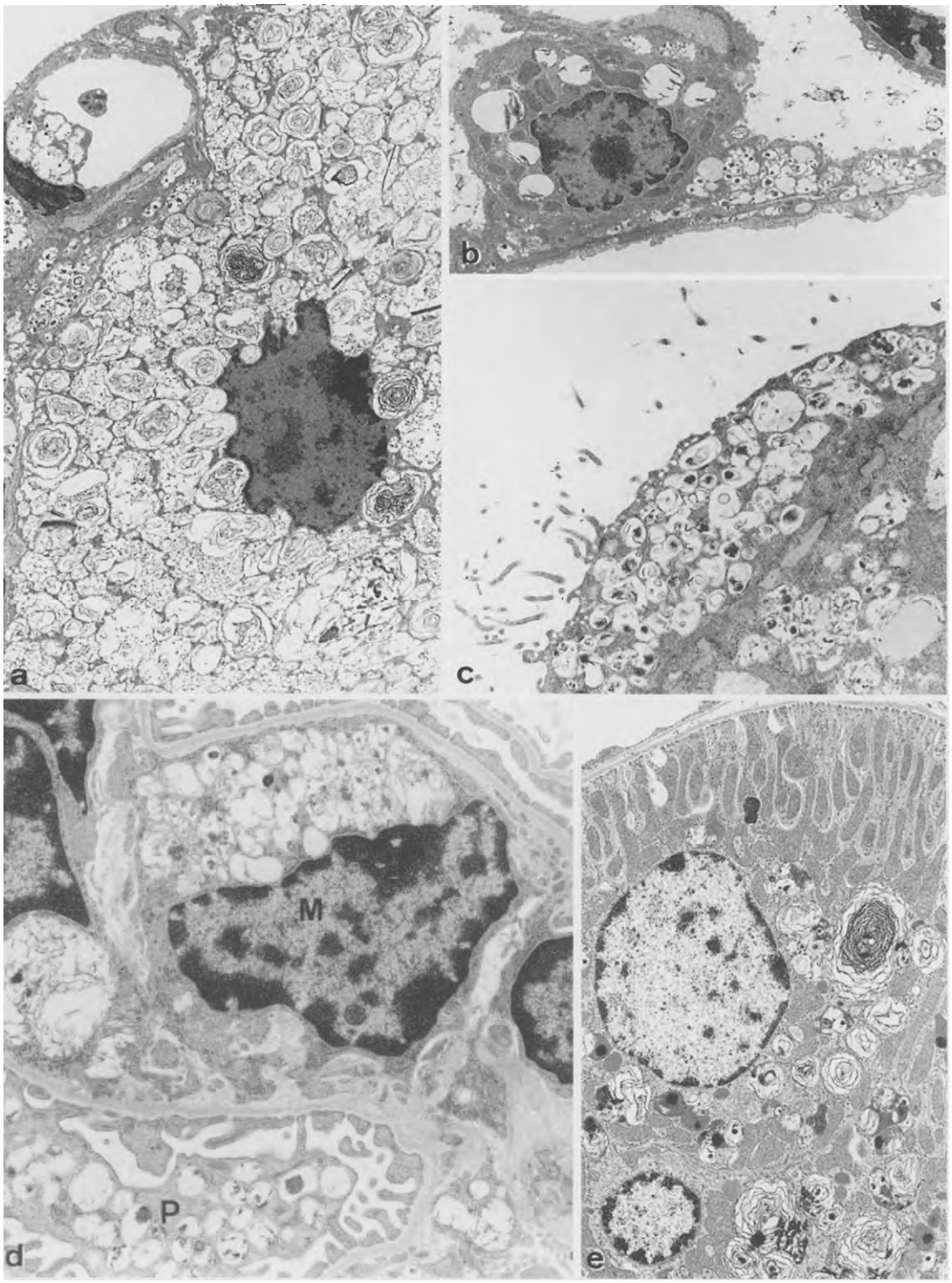

Fig. 4. Lung and kidney of the 140-day-old animal: **a)** Large macrophage occluding an alveolus that displays numerous inclusions with mostly coiled membranous material of varying density. Upper left corner of the picture: Small capillary with multivesicular inclusions in the cytoplasm of an endothelial cell and narrowing of the vascular lumen. **b)** Unremarkable pneumocyte, type II next to the cytoplasm of pneumocytes type I, lining the alveolar wall that discloses numerous vesicular and vesiculo-granular inclusions. **c)** Ciliated epithelium of a bronchiole with partly confluent vesicular and vesiculo-granular inclusions along with similar multivesicular bodies in the underlying connective tissue. **d)** Part of kidney glomerulus with mostly vesicular and vesiculo-granular membrane-bound bodies in mesangial cells (M) and podocytes (P). **e)** Distal tubule epithelium of kidney with numerous inclusions, containing coiled membranous material of varying density. a: ×5,400; b, e: ×6,000; c, d: ×13,000.

Discussion

A comparative evaluation of the pathology in human NP-A with the lesions in the transgenic mouse model investigated here, yielded some interesting aspects. These animals displayed identical clinical symptoms compared to the initial series investigated [26]. Moreover, our light microscopical findings in visceral organs of mice suffering from an advanced stage of this disorder were in general keeping with those, reported in the aforementioned study. However, our systematical ultrastructural investigation enabled a closer insight into the cellular alterations associated with NP-A and, therefore, extended former investigations in the field of storage disorders in a significant way.

Organs that contain multiple cells of the mononuclear-macrophage system [18, 35], like bone marrow and spleen are known to display an early and most severe involvement with regard to disorders of the NP-group [32]. For this reason and also because of its easy availability, the bone marrow yields an early approach for the diagnosis of a lipidosis in man [20, 40]. Occurrence of foam cells was reported for both aSmase knock-out mouse models [15, 26]. In agreement with findings in the model presented here, the extent of foam cell infiltration varies with the duration of the disease in man [3]. Thus, repeatedly performed bone marrow biopsies may evolve as a diagnostic necessity and could also be helpful to monitor the disease progression.

Hepatosplenomegaly with spleen sizes as much as ten times of normal and enlargement of liver from 1.5- to two-fold were well-known features of human NP-A [8, 12, 17, 37]. This is in good agreement with an increase of the wet weight of spleen about twice and of liver about 1.5 times in NP-mice with a final stage of the disorder compared with age and sex-matched wild-type mice [26]. Moreover, hepatosplenomegaly, in particular enlargement of the spleen was also reported for NP-A-like disorders resulting from spontaneous mutations in a poodle dog [4] and in Siamese cats [31] while it was not evident in a Balinese cat [1] and the aSmase knock-out mouse model, established by Horinouchi and coworkers [15]. Histologically, occurrence of foamy macrophages in spleen was a common finding in all aforementioned animal models and in case reports of NP-A in man [7, 8, 12]. Similar as described for the aSmase$^{-/-}$ knock-out mice under study, foam cells in human NP-A were localized in both red and white pulp of the spleen with a certain predominance in sinusoids of the red pulp [8, 11, 20]. This is in keeping with findings reported in a feline lipidosis resembling NP-A [1]. Moreover, lymphocyte affection is a well-known phenomenon for several storage disorders in man, including NP-A [8, 16, 20].

Liver tissue pathology in full-blown cases of human NP-A discloses a major involvement of the monocyte-macrophage system (Kupffer cells and portal macrophages) and of hepatocytes [10, 37]. Clusters of large foam cells often fill the sinusoid lumen and occlude the space of Disse [7]. These alterations are identical with the pathology of the mouse model investigated here. Mononuclear cells with foamy cytoplasm were also described in the canine [4] and feline [31] models of this disease and ultrastructural investigations in a Balinese cat revealed large numbers of membranous inclusions [1].

Single studies of the gastrointestinal manifestations in human NP-A reported a normal villous structure of small bowel along with a massive foam cell infiltration of the lamina propria [9, 14]. These changes are almost in line with the findings reported here. The heavy infiltration resulting in a blockage of the intestinal wall is assumed to be an early cause of malabsorption in NP disease. Enteropathy may be even aggravated by dysfunctions of other organs, functionally involved in normal digestive and absorptive processes, e.g. liver damage [14].

Foam cell infiltration of alveoli of the lungs is a well-known feature in human NP-A [20, 30, 37]. As a roentgenographic expression of the pathological accumulation of stored material, a diffuse reticular infiltration was demonstrated [13]. A widespread involvement of the lungs was also reported in the canine [4] and feline [1, 31] models of this disorder. On the other hand, there is only little information available concerning ultrastructural alterations of lungs in the NP disorder. The investigations reported here are almost identical with recent findings in a murine model of NP-C. In this model an affection of alveolar macrophages and endothelial cells along with ciliated epithelia of bronchioles was observed. Moreover, vesiculo-granular structures were visible in type I pneumocytes, whereas pneumocytes of the type II were completely unremarkable [23]. Lamellar bodies, being rich in phospholipides are a common finding in the latter type of pneumocytes. These constituents can be delivered to the alveolar surface to built up a smooth molecular film of a surface active agent, the so-called surfactant [22].

Morphological changes in the kidney were reported in various storage disorders including NP disease [8, 29]. In NP-A, these involved both, the glomeruli and the tubular epithelium with occurrence of foam cells either resulting from foamy transformation of renal cells or from blood born dissemination [28, 29]. In agreement with these findings in man, our results clearly indicate renal involvement of both the glomeruli and the tubular system in the aSmase$^{-/-}$ knock-out mouse. They revealed mostly vesicular or vesiculo-granular inclusions in cells of the glomeruli and a predominance of typical whirl-like lamellar structures in epithelial cells of the tubular system (Fig. 4d, e). Similarly an ultrastructural examination of kidney in an aSmase-deficient Balinese cat disclosed membrane-bound bodies of different appearance

in glomeruli, proximal and distal tubules and vascular elements [1]. Inclusions in a Siamese cat with this disorder were more uniform, disclosing a lamellar appearance in all renal cells studied except for endothelial cells that were not affected [6]. Contrasting this situation, the kidney of a poodle dog with aSmase deficiency showed no remarkable findings at all [4].

Storage phenomena in human endothelial cells of small vessels are described in the brain and in visceral organs [11, 20, 30, 37]. In keeping with these observations we recently reported gross storage phenomena in small vessels of the nervous system in the aSmase knock-out mouse [19]. Our results presented here disclosed similar inclusions in vascular endothelial cells of visceral organs. An affection of endothelial cells in most visceral organs was also described in the feline models of this disorder [1, 31]. However, the ultrastructure showed large membranous whorls [1], rather than vesicular and vesiculo-granular structures as detected in our mouse model.

A certain heterogeneity of the ultrastructural appearance of lysosomal storage was evident in this study. This peculiar feature applied to different visceral organs, different cells within one visceral organ as well as different lysosomes within one cell. It regarded both, the size of vacuoles and morphology of storage material. The size of membrane-bound inclusions ranged from small vesicles frequently detected in endothelial cells (Fig. 4a) to huge fusion bodies containing pleomorphic membranous deposits (Fig. 2b and 3c). Similar to our animal model ample evidence has also been accumulated about the lysosomal pleomorphism in human NP-A [11]. Considering this aspect, an approach using the ultrastructural appearance of storage material alone as a diagnostic tool to further classify lipidoses [34] seems to be of limited value. On the other hand, electron microscopy is generally regarded as a powerful tool in detecting minimal lysosomal storage [11].

In conclusion, the aSmase$^{-/-}$ knock-out mouse model investigated here discloses a generalized storage disorder that involves not only elements of the mononuclear-macrophage system, but additionally a variety of parenchymal cells in the visceral organs. By a comparative study with human NP-A, mounting evidence has been provided that it presents an animal model which closely resembles the corresponding disorder in man. For this reason, the aSmase$^{-/-}$ mouse model should be regarded as a reliable tool to further investigate the clinical and pathological progression of the disease and to establish new therapeutic strategies, particularly in gene therapy [24]. Moreover, these mice offer an unique opportunity to define the role of sphingomyelinases in signal transduction more clearly [33]. In this regard, experimental evidence was provided recently, that aSmase is not involved in the tumor necrosis factor α induced activation of nuclear transcription factor κB [41].

Acknowledgements: The authors gratefully acknowledge the technical assistance of Mrs. E. Varus and Mrs. M. Düker.

References

1. Baker HJ, Wood PA, Wenger DA, Walkley SU, Inui K, Kudoh T, Rattazzi MC, Riddle BL (1987) Sphingomyelin lipidosis in a cat. Vet Pathol *24*: 386–391
2. Brady RO, Kanfer JN, Mock MB, Fredrickson DS (1966) The metabolism of sphingomyelin. II. Evidence of an enzymatic deficiency in Niemann-Pick disease. Proc Natl Acad Sci USA *55*: 366–369
3. Brady RO (1983) Sphingomyelin lipidoses: Niemann-Pick disease. In: Stanbury JB, Wyngaarden JB, Fredrickson DS, Goldstein JL, Brown MS (Eds) The metabolic basis of inherited disease, pp. 831–841. McGraw-Hill, Inc, New York
4. Bundza A, Lowden JA, Charlton KM (1979) Niemann-Pick disease in a poodle dog. Vet Pathol *16*: 530–538
5. Carstea ED, Morris JA, Coleman KG, Loftus SK, Zhang D, Cummings C, Gu J, Rosenfeld MA, Pavan WJ, Krizman DB, Nagle J, Polymeropoulos MH, Sturley SL, Ioannou YA, Higgins ME, Comly M, Cooney A, Brown A, Kaneski CR, Blanchette-Mackie EJ, Dwyer NK, Neufeld EB, Chang T-Y, Liscum L, Strauss III JF, Ohno K, Zeigler M, Carmi R, Sokol J, Markie D, O'Neill RR, van Diggelen OP, Elleder M, Patterson MC, Brady RO, Vanier MT, Pentchev PG, Tagle DA (1997) Niemann-Pick C1 disease gene: homology to mediators of cholesterol homeostasis. Science *277*: 228–231
6. Castagnaro M, Alroy J, Ucci AA, Glew RH (1987) Lectin histochemistry and ultrastructure of feline kidneys from six different storage diseases. Virch Arch B *54*: 16–26
7. Chamlian A, Gulian JM, Benkoel L (1986) Ultrastructural and enzyme histochemical study of liver in Niemann-Pick disease. Cell Mol Biol *32*: 273–282
8. Crocker AC, Farber S (1958) Niemann-Pick disease: a review of eighteen patients. Medicine *37*: 1–95
9. Dinari G, Rosenbach Y, Grunebaum M, Zahavi I, Alpert G, Nitzan M (1980) Gastrointestinal manifestations of Niemann-Pick disease. Enzyme *25*: 407–412
10. Elleder M, Smid F, Harzer K., Cihula J (1980) Niemann-Pick disease. Analysis of liver tissue in sphingomyelinase deficient patients. Virch Arch A *385*: 215–231
11. Elleder M (1989) Niemann-Pick disease. Pathol Res Pract *185*: 293–328
12. Fredrickson DS (1966) Sphingomyelin lipidosis: Niemann-Pick disease. In: Stanbury JB, Wyngaarden JB, Fredrickson DS (Eds) The metabolic basis of inherited disease, pp. 586–617. McGraw-Hill, Inc, New York
13. Grünebaum M (1976) The röntgenographic findings in the acute neuronopathic form of Niemann-Pick disease. Br J Radiol *49*: 1018–1022
14. Hager-Malecka B, Szczepanski Z, Karczewska K, Sonta-Jakimczyk D (1973) Enteropathy in Niemann-Pick disease. Z Kinderheilk *115*: 71–75
15. Horinouchi K, Erlich S, Perl DP, Ferlinz K, Bisgaier CL, Sandhoff K, Desnick RJ, Stewart CL, Schuchman EH (1995) Acid sphingomyelinase deficient mice: a model of

types A and B Niemann-Pick disease. Nat Genet *10*: 288–293
16. Ikeda K, Goebel HH, Burck U, Kohlschütter A (1982) Ultrastructural pathology of human lymphocytes in lysosomal disorders: a contribution to their morphological diagnosis. Eur J Pediatr *138*: 179–185
17. Ivemark BI, Svennerholm L, Thoren C, Tunell R (1963) Niemann-Pick disease in infancy: report of two siblings with clinical, histologic and chemical studies. Acta Paediatr *52*: 391–404
18. Johnston RB Jr (1988) Current concepts: immunology. Monocytes and Macrophages. N Engl J Med *318*: 747–752
19. Kuemmel TA, Schroeder R, Stoffel W (1997) Light and electron microscopic analysis of the central and peripheral nervous systems of the acid sphingomyelinase-deficient mice resulting from gene targeting. J Neuropathol Exp Neurol *56*: 171–179
20. Lake BD (1994) Lysosomal and peroxisomal disorders. In: Adams JH, Duchen LW (Eds) Greenfield's neuropathology, pp 709–810. Hodder and Stoughton, London
21. Loftus SK, Morris JA, Carstea ED, Gu JZ, Cummings C, Brown A, Ellison J, Ohno K, Rosenfeld MA, Tagle DA, Pentchev PG, Pavan WJ (1997) Murine model of Niemann-Pick C disease: mutation in a cholesterol homeostasis gene. Science *277*: 232–235
22. Manabe T (1979) Freeze-fracture study of alveolar lining layer in adult rat lungs. J Ultrastruct Res *69*: 86–97
23. Manabe T, Yamane T, Higashi Y, Pentchev PG, Suzuki K (1995) Ultrastructural changes in the lung in Niemann-Pick type C mouse. Virch Arch *427*: 77–83
24. Miranda SRP, Erlich S, Visser JWM, Gatt S, Dagan A, Friedrich Jr VL, Schuchman EH (1997) Bone marrow transplantation in acid sphingomyelinase-deficient mice: engraftment and cell migration into the brain as a function of radiation, age, and phenotype. Blood *90*: 444–452
25. Miyawaki S, Mitsuoka S, Sakiyama T, Kitagawa T (1982) Sphingomyelinosis, a new mutation in the mouse: a model of Niemann-Pick disease in humans. J Hered *73*: 257–263
26. Otterbach B, Stoffel W (1995) Acid sphingomyelinase-deficient mice mimic the neurovisceral form of human lysosomal storage disease (Niemann-Pick disease). Cell *81*: 1053–1061
27. Pentchev PG, Gal AE, Booth AD, Omodeo-Sale F, Fouks J, Neumeyer BA, Quirk JM, Dawson G, Brady RO (1980) A lysosomal storage disorder in mice characterized by a dual deficiency of sphingomyelinase and glucocerebrosidase. Biochim Biophys Acta *619*: 669–679
28. Pick L (1933) Niemann-Pick's disease and other forms of so-called xanthomatosis. Am J Sci *185*: 601–616
29. Rosenmann E, Aviram A (1973) Glomerular involvement in storage diseases. J Pathol *111*: 61–64
30. Schuchman EH, Desnick RJ (1995) Niemann-Pick disease types A and B: acid sphingomyelinase deficiencies. In: Scriver CR, Beaudet AL, Sly WS, Valle D (Eds) The metabolic and molecular basis of inherited disease, pp 2601–2624. McGraw-Hill, Inc, New York
31. Snyder SP, Kingston RS, Wenger DA (1982) Animal model of human disease. Niemann-Pick disease: sphingomyelinosis of Siamese cats. Am J Pathol *108*: 252–254
32. Spence MW, Callahan JW (1989) Sphingomyelin-Cholesterol lipidoses: The Niemann-Pick group of diseases. In: Scriver CR, Beaudet AL, Sly WS, Valle D (Eds) The metabolic basis of inherited disease, pp 1655–1676. McGraw-Hill, Inc, New York
33. Spiegel S, Foster D, Kolesnick R (1996) Signal transduction through lipid second messengers. Curr Opin Cell Biol *8*: 159–167
34. Takahashi K, Naito M (1985) Lipid storage disease: Part II. Ultrastructural pathology of lipid storage cells in sphingolipidoses. Acta Pathol Jpn *35*: 385–408
35. Van Furth R (1989) Origin and turnover of monocytes and macrophages. Curr Top Pathol *79*: 125–150
36. Vanier MT, Rodriguez-Lafrasse C, Rousson R, Duthel S, Harzer K, Pentchev PG, Revol A, Louisot P (1991) Type C Niemann-Pick disease: biochemical aspects and phenotypic heterogeneity. Dev Neurosci *13*: 307–314
37. Volk BW, Adachi M, Schneck L (1972) The pathology of sphingolipidoses. Semin Hematol *9*: 317–348
38. Walkley SU, Baker HJ (1984) Sphingomyelin lipidosis in a cat: golgi studies. Acta Neuropathol *65*: 138–144
39. Wenger DA, Sattler M, Kudoh T, Snyder SP, Kingston RS (1980) Niemann-Pick disease: a genetic model in Siamese cats. Science *208*: 1471–1473
40. Ziyeh S, Harzer K (1994) Bone marrow cytological storage phenomena in lipidoses. Eur J Pediatr *153*: 224–233
41. Zumbansen M, Stoffel W (1997) Tumor necrosis factor α activates NF-κB in acid sphingomyelinase-deficient mouse embryonic fibroblasts. J Biol Chem *272*: 10904–10909

Received: October 10, 1997
Accepted in revised form: November 11, 1997

Address for correspondence: Jürgen Thiele M.D., Institute of Pathology, University of Cologne, Joseph-Stelzmann-Str. 9, D - 50924 Cologne. Phone: ++49(0)221-478 5008, Fax: ++49(0)221-478 6360